Construction and Building Materials 314 (2022) 125574

Contents lists available at ScienceDirect

Construction and Building Materials

journal homepage: www.elsevier.com/locate/conbuildmat

Enhancing the thermal performance of Class F fly ash-based geopolymer by sodalite

K.M. Klima [a], K. Schollbach [a], H.J.H. Brouwers [a], Qingliang Yu [a,b,*]

[a] Department of the Built Environment, Eindhoven University of Technology, Eindhoven 5600 MB, the Netherlands
[b] School of Civil Engineering, Wuhan University, Wuhan 430072, PR China

ARTICLE INFO

Keywords:
Class F fly ash
Geopolymer
Sodalite
High temperature resistance
Zeolite geopolymer composite

ABSTRACT

Class F Fly ash-based geopolymers are prone to various high-temperature phenomena, such as cracking, spalling, and thermal shrinkage. Here we study the effect of enriching the Class F fly ash with synthetic sodalite phase in order to enhance the thermal properties of the formed geopolymer. The morphological changes, compositional changes, alterations in porosity, high-temperature gel behaviour, and the effect of sodalite on the deformation of the material after thermal exposure up to 1000 °C are investigated by a multiple-analytical approach. Results indicate that adding 5 wt% of the sodalite phase enhances considerably high-temperature performance by inducing phase formation, including anorthoclase, wollastonite, and leucite. Besides, the sodium-bearing sodalite phases lowered the glass transition temperature, thanks to the formation of a mixed K-Na glass phase. Moreover, thermal shrinkage at high temperature is substantially reduced by the addition of sodalite, suggesting its function as a skeletal reinforcement.

1. Introduction

Increased awareness and demand for fire safety of buildings are promoting research on fire-resistant materials, especially inorganic-based materials. One recent focus is geopolymers thanks to their high corrosion (acidic attack) and high-temperature resistance [1–3], in addition to their considerably eco-friendly characteristics. Geopolymers are formed by alkaline activation of aluminosilicate sources such as fly ash [4–5]. The lower water demand of fly ash-based geopolymers benefits in minimizing the damage caused by water evaporation during high-temperature exposure. Furthermore, compared to metakaolin-based geopolymers continuous sintering of fly ash particles triggered particle binding and strength increase with temperature increase. The aluminosilicate gel contributes essentially towards the high-temperature performance. However, geopolymers also release the physically and chemically bound water at elevated temperatures, which can destabilize the material structure and cause the thermal shrinkage and crack formation [6]. Besides, the vapor pressure produced by both the physically and chemically absorbed water within the matrix will attempt to escape at elevated temperature. Thus, the level of thermally-induced damage is highly dependent on the pore structure of the material. Moreover, the research conducted by Ozawa and Shaikh [7] showed that pure fly ash-based geopolymer did not exhibit the abrupt decrease in vapour pressure reported in cement-based and fly ash/slag-based materials, resulting in spalling and cracks, which may also demonstrate the advantageous utilization of fly ash in synthesis of geopolymer. Taking into account the enormous influence of the microstructure on geopolymer thermal degradation, the research focusing on the improvement of the matrix in order to address these issues is of great significance.

Currently, different approaches have been taken to minimize shrinkage by enriching geopolymer with different fillers [8–12], as well as, to change the microstructure by optimizing the pore structure. Direct foaming [13–16] or sacrificial filler [15,17–18] are two methods for generating highly porous geopolymers. Those methods are effective; however, a substantial decrease in material strength is observed across the entire temperature range, as well as increased shrinkage induced by viscous flow at above 600 °C [19]. Several recent studies focus on hybrid geopolymers due to their unique room and high-temperature performance. This hybrid form of geopolymers can be produced by incorporating organic compounds, such as organic resin [20], or inorganic compounds, such as highly crystalline zeolites [8]. The latter approach provides an alternative path to alter the pore structure of geopolymer composite.

Zeolites have been reported for various applications such as

* Corresponding author at: Department of the Built Environment, Eindhoven University of Technology, Eindhoven 5600 MB, the Netherlands.
E-mail address: q.yu@bwk.tue.nl (Q. Yu).

https://doi.org/10.1016/j.conbuildmat.2021.125574
Received 20 June 2021; Received in revised form 24 October 2021; Accepted 4 November 2021
Available online 14 November 2021

adsorption of heavy metals for disposal [8,21], as a geopolymer precursor [22–23] or as a filler to improve srength performance [24]. Zeolites are aluminosilicates with an open tetrahedral framework that results in considerable open micropores in the structure and allows ion exchange and reversible dehydration. These characteristics could provide geopolymers with defined pathways that make the dehydration at elevated temperatures possible without causing structural damage.

Several zeolites are known to maintain their crystal structure at elevated temperatures, for example, those with a sodalite, analcime, or faujasite framework [25]. Among these zeolites, sodalite ($(M_8(AlSiO_4)_6X_2)$, where M is a cation (e.g., Na^+, Ca^{2+}) and X is an anion (e.g., Cl^-, I^-, OH^-)) is the most promising candidate, due to its high temperature [25–26] and high alkaline stability [27]. Moreover, the synthesis proposed by Franus et al. [28] allows for the reproducible sodalite synthesis from Class F fly ash, which can also serve as a solid precursor for geopolymers. However, there is little information about the high-temperature behaviour of the zeolites themselves. For instance, its path of transformations, the ability to undergo amorphization, recrystallization, dealumination during thermally-induced dehydroxylation [21,29], and large volumetric phase changes have not been systematically studied.

The main objective of this article is to evaluate whether ex-situ sodalite enrichment can influence the performance of fly ash-based geopolymer at high temperature and the associated behaviour related to the phase composition and microstructure alteration. We firstly discussed the hydrothermal synthesis of sodalite from fly ash, as well as the identification of its structure and quantitative analysis of the resulting product using Rietveld refinement method. The synthesized sodalite was then added to the geopolymer paste and the quantitative phase analysis was performed to investigate the evolution of the phase composition after high-temperature exposure, the stability of sodalite in the geopolymer matrix, and its influence on the formation of new phases. Besides, thermal analysis (TG-DSC) was employed to monitor the reactions as well as melting caused by the elevated temperature. Moreover, the effects of sodalite on the evolution of the strength, pore structure, as well as gel morphology under high-temperature conditions, were investigated. The investigation revealed that sodalite can play two roles in geopolymers, under both low (up to 600 °C) and high temperature (>600 °C) environments. At low temperature, attributed to its porous structure, in combination with the pores in geopolymers, effective paths can be created for escaping water, which helps to reduce or avoid water vapor pressure-induced thermal spalling damages. In terms of high temperatures, above 600 °C, sodalite would act as a backbone for amorphous geopolymer gels, which would lose stability due to thermal shrinkage and melting.

2. Methodology

2.1. Material and reagents

In this study, Coal Combustion Fly Ash class F was used as the solid precursor both for zeolite synthesis and geopolymer preparation. Sodium hydroxide pellets and sodium chloride solution (3 mol/l) were used (Sigma-Aldrich Chemie GmbH, analytical purity). The composition of fly ash was determined by X-ray fluorescence spectrometry (XRF; PANalytical Epsilon 3) with the application of fused beads (Table 1).

The Si/Al molar ratio based on XRF and XRD analysis revealed the potential reactivity of the analyzed system, an interesting phenomenon related to a similar value of Si/Al ratio between amorphous content and XRF measurement. It is assumed in this study that an amorphous part is considered as a reactive part of the raw material (Table.2).

2.2. Procedure of sodalite synthesis and its characterization

The synthesis of sodalite was performed by mixing 60 g of Coal Combustion Fly Ash with 0.8 l of sodium hydroxide solution ($C_M = 5$ mol/l) and 0.5 l of sodium chloride solution ($C_M = 3$ mol/l). This methodology is based on Franus et al. [28], which, by the authors, is considered to be one of the most practical ways to obtain the sodalite phase from Coal Combustion Fly Ash. The synthesis was carried out using a round bottom flask (volume 2 L) with a reflux condenser to avoid evaporation and keep a constant liquid-to-solid ratio (L/S). The slurry was mixed constantly using a magnetic stirrer with temperature control. Heating was performed on the heating plate with oil bath. The synthesis conditions include 22 h of stirring at a temperature of 105 °C. Table 3 shows the composition of the oxides and a significant reduction of silica content was observed due to the partial dissolution of soluble Si in NaOH solution, which resulted in a lower SiO_2/Al_2O_3 ratio. Furthermore, the presence of sodium and chloride is associated with the reaction environment. Fig. 1 shows the reaction product where sodalite formed clusters and precipitated on the fly ash spherical particles, and the formation of these aggregates has been observed in the literature [30–31]. The crystal size based on SEM was estimated to be ~ 4 μm and the BET surface area was calculated to be 24.15 m^2/g. The pore width with the range > 3.5 nm and the mean pore width was established at 14.6 nm which defined sodalite-rich material as *meso*-macroporous with a significant contribution of pores size 4 nm as visible in Fig. 2. The broad pore size distribution between 4 and 100 nm is in agreement with previous studies regarding sodalite crystals synthesis [31–33].

Fig. 3 shows the XRD patterns of Class F Fly Ash and sodalite-rich product. The phase composition of fly ash revealed the majority of amorphous phase (78.1 wt%) and typical crystalline phases such as quartz, mullite, and iron oxides with a minor content of additional phases (see Table A in Appendix). The diffractogram of the sodalite-rich product shows that the synthesis was indeed successful and that sodalite is the main component (36.3 wt%). Noteworthy, the ash has not undergone any additional treatments to remove impurities. The sodalite phase includes both chlorosodalite (30.5 wt%) and hydroxysodalite (5.8 wt%) which is a typical phenomenon of hydrothermal synthesis. It should be mentioned that the term sodalite in this study describes a mixture of chloro- and hydroxy- sodalite.

IR spectroscopy has been used to identify the structures of the synthesized sodalite. Fig. 4 shows the FT-IR spectrum with the characteristic absorption bands highlighted, which allowed the material to be classified as aluminosilicate sodalite spectrums based on the standard building structure units, confirming the formation of chlorosodalite [34].

Table 2
Fly ash reactivity based on amorphous Si/Al content

	Moles of Si per 100 g of FA	Moles of Al per 100 g of FA	Si/Al molar ratio
Total content (XRF)	0.8538	0.5281	1.62
Crystalline content (XRD)	0.1959	0.1315	1.49
Amorphous content	0.6579	0.3966	1.66

Table 1
Oxide Composition of Fly Ash.

Component	SiO_2	Al_2O_3	Fe_2O_3	CaO	MgO	K_2O	P_2O_5	TiO_2	SO_3	SrO	Other oxides	LOI
Amount (%)	51.30	26.92	7.61	5.20	1.10	1.46	0.60	1.43	0.34	0.17	0.25	3.62

Table 3
Oxide Composition of the reaction product

Component	SiO_3	Al_2O_3	Na_2O	Fe_2O_3	CaO	Cl	MgO	TiO_2	SO_3	P_2O_5	K_2O	Others	LOI
Amount (% by mass)	31.8	25.6	14.3	6.9	5.4	1.3	1.2	1.5	0.3	0.2	0.1	0.3	12.5

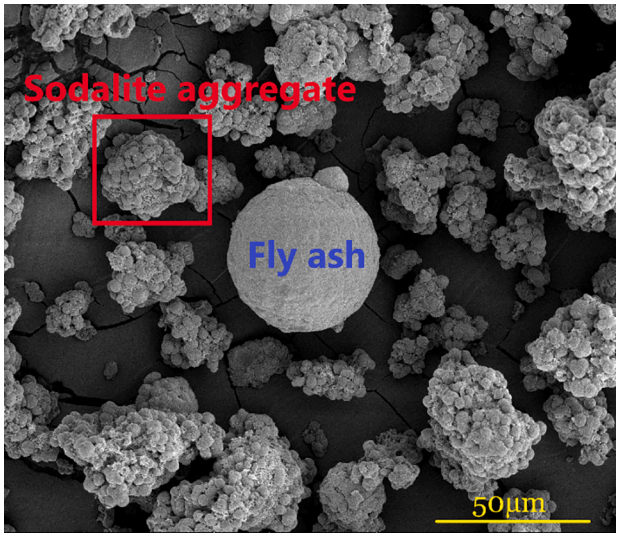

Fig. 1. SEM of hydrothermal reaction product.

2.3. Mix design and sample preparation

The alkaline solution for the geopolymer was prepared by mixing potassium hydroxide pellets (VWR Life Science, reagent grade) and potassium silicate solution (WHC GmbH, K_2O 8 %, SiO_2 20.8 %, 72.8 % H_2O by mass) to obtain a SiO_2/K_2O ratio of 1.4. The selection of the silica modulus was based on previous research [35].

The sample composition is presented in Table 4. The amounts of zeolite added, 3.5 wt% and 5 wt%, are based on work by Krivenko and Kovalchuk [36], who observed that the content of zeolite between 2.5 and 10 wt. % performs well under high-temperature conditions. Prior to the application, the sodalite was pre-mixed with deionized water to avoid problems with workability due to the high-water adsorption [37].

Mixing the fly ash with a potassium-based activator for 3 min was preceded by a one-minute mixing of the dry fly ash for homogenization. Then zeolite slurry was added to the fresh paste. This blend was mixed for a further two minutes to obtain a homogeneous mixture with the evenly dispersed sodalite. The prepared pastes were cast into moulds with the dimensions of 40 mm × 40 mm × 160 mm. The samples were first sealed cured at ambient temperature for 24 h [38] and then cured at an elevated temperature of 60 °C for 24 h in the climate chamber (80 % RH) to facilitate geopolymeric reaction [39]. Next, the samples were sealed in plastic foil and stored at room temperature until the testing time.

2.4. Characterization techniques

The phase analyses of both synthetic zeolites and geopolymer before and after high-temperature exposure were performed by XRD measurements. Powder samples of geopolymers were back loaded in the sample holders and measured with a Bruker D4 equipped with a LynxEye detector. The range of 10–80° (2θ) was measured with a 0.02° step size using a Co-Tube. Qualitative analysis was carried out with X'Pert HighScorePlus 2.2 (PANalytical), while quantitative X-ray diffraction analysis (QXDA) with Rietveld refinement was conducted by the software Topas Academic v4.1. Silicon powder was used as an internal standard. The crystal structures with ICSD number are listed in Table 5.

After 28 days of curing, mercury intrusion porosimetry (MIP) tests were carried out on the paste samples. The cubic pieces were crushed to obtain particles with a size of 3 mm, they were immersed in isopropanol to stop the hydration and dried in a desiccator for 3 days [40]. The measurements were conducted using an AutoPore IV Series Porosimeter. The applied contact angle of mercury was 130° and the surface tension 485 dynes/cm.

The thermal behaviour of geopolymer specimens at the age of 28 days was evaluated using a STA F1 Jupiter analyzer (Netzsch Instruments). The measurement was carried out from 40 to 1000 °C at a heating rate of 10 °C/min in nitrogen atmosphere with a flow of 20 ml/min. For the DSC analysis, additional measurements were included with a variation of heating rate from 5 to 20 °C/min in order to confirm the glass transition temperatures.

The high-temperature tests were performed on samples at the age of

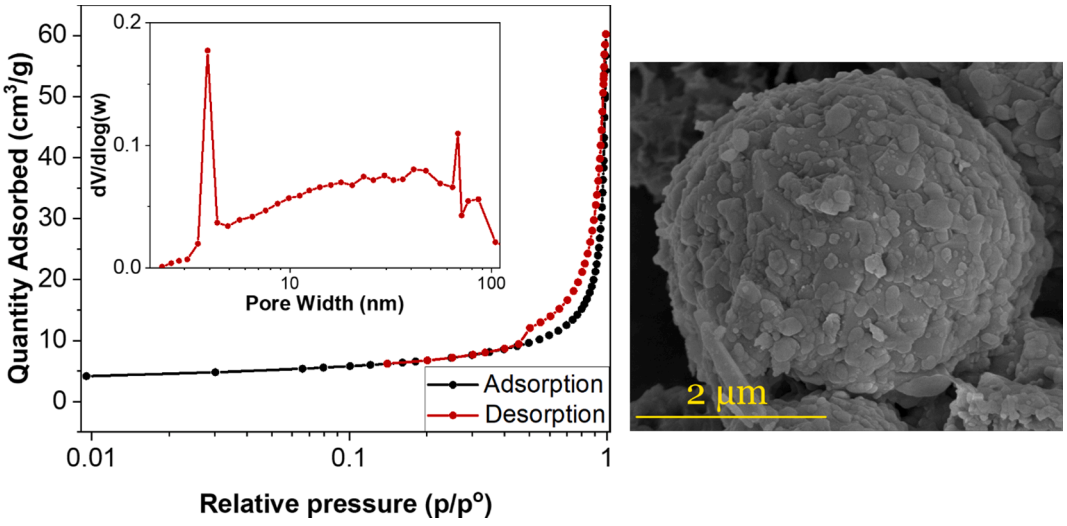

Fig. 2. SEM and BET analysis of sodalite crystals synthesized from fly ash.

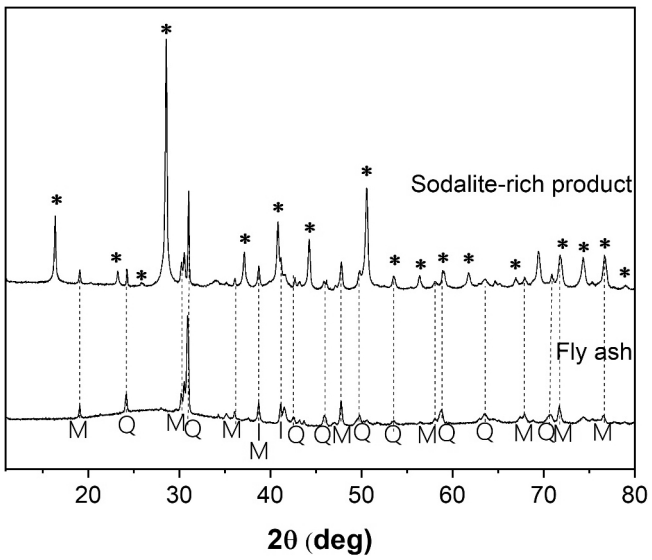

Fig. 3. XRD diffractograms of the fly ash and material after hydrothermal synthesis: sodalite-rich product. Legend: (* -Sodalite; Q – quartz; M – Mullite; I – Iron (III) oxide, *-Sodalite; (detailed phase analysis shown in Table A (Appendix)).

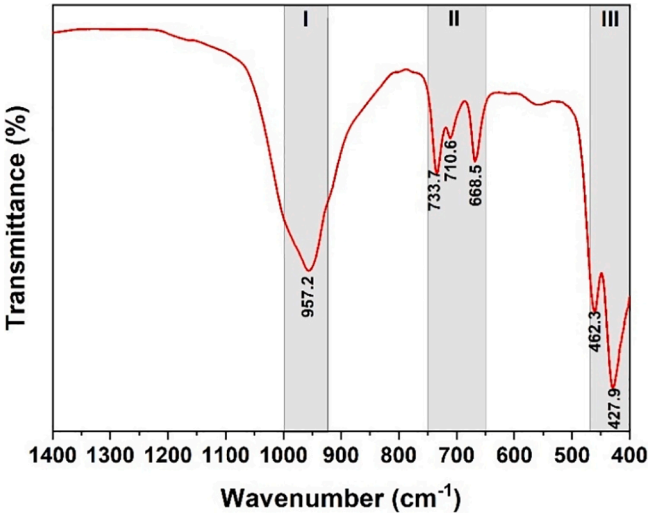

Fig. 4. FT-IR of sodalite-enriched material. Region I represent υ_{as} (Al-O-Si) ~ 957 cm^{-1}; region II υ_s (Al-O-Si) ~ 650–750 cm^{-1} and δ (O-T-O) ~ 460–400 cm^{-1}.

Table 4
The specific composition ratios of geopolymer pastes.

Sample	Fly ash wt. %	Sodalite-rich material		Water/ Binder*	K_2O/ Binder	SiO_2/ K_2O
		In total	Pure sodalite			
G-FA	100	–	–	0.17	5.5	1.4
G-S1	85	15	3.5	0.23	5.5	1.4
G-S2	78.5	21.5	5.0	0.29	5.5	1.4

*includes water used for pre-treatment of sodalite-rich material.

28 days. The samples were placed in a muffle furnace at room temperature and heated up to the temperatures 400, 600, 800 or 1000 °C respectively at a heating rate of 10 °C/min and exposed at specific temperatures for 1 h. This was followed by short water-quenching during the first 15 min after 1-hour exposure and further air-quenching.

Table 5
List of XRD patterns used in qualitative and quantitative analysis with ICSD number.

Phase name		Formula	ICSD number
Quartz		SiO_2	27831
Mullite		$Al_{1.83}O_{4.85}Si_{1.08}$	43298
Magnetite		Fe_3O_4	31156
Hematite		Fe_2O_3	15840
Maghemite		γ-Fe_2O_3	87121
Sodalite group	Sodalite	$Al_6Cl_2Na_8O_{24}Si_6$	98807
	Hydroxysodalite	$Na_8(Si_6Al_6O_{24})(OH)_2(H_2O)_2$	412496
Leucite		$Al_{0.96}KO_6Si_{2.04}$	9826
Anorthoclase		$AlK_{0.333}Na_{0.667}O_8Si_3$	31180
Hallite potassian		$ClK_{0.0997}Na_{0.9003}$	28947
Anatase		O_2Ti	63711
Periclase		MgO	26958
Wollastonite-1A		Cao_3Si	23567
Pyrrhotite		Fe_7S_8	42491
Calcite		$CCaO_3$	40107
Nepheline		$Al_4KNa_3o_{16}Si_4$	26007

SEM analyses were performed by using a Phenom ProX scanning electron microscope with a BSD detector to investigate the geopolymeric gel changes after high-temperature exposure. Micrographs were recorded at 10.00 kV, while the EDX analysis at 15 kV. The core samples were obtained by cutting and further polishing of the samples. The specimens were sputtered with gold (Emitech K550X sputter coater current 60 mA, coating time 30 s). Additionally, optical microscope ZEISS Axio Observer with lens turret 5x and 10x was applied to support SEM findings and observe colour changes of the sample after 1000 °C exposure.

The volumetric changes were measured on the prisms before and after exposure to high temperature, expressed in percentage. The values are an average of three measurement per mix and temperature setting using digital caliper to find the length, width, and height of each prism and calculate the total volume. The compressive strength of the samples after 28 days and high-temperature exposure was determined according to the standard EN 196–1 [41] as an average value of six measurements for each mix.

3. Results and discussion

3.1. Phase characterization

Fig. 5 shows the diffractograms of the FA geopolymer containing 3.5 and 5.0 wt% of sodalite in comparison with sodalite-free geopolymer before heating. All the 3 samples were cured for 28 days. As can be seen, the addition of sodalite has very little influence on the crystalline structures. G-S2 paste was characterized by a lower content of the amorphous phase 76.7 wt% compared to the reference paste G-FA 82.3 wt%; however, the general composition stayed similar with the only exception of the presence of sodalite for sample G-S1 and G-S2. To investigate the composition of pastes, the phases were identified and quantified by QXRD (Table A in Appendix). At ambient temperature, mostly amorphous phases were formed, as a result of fly ash particles dissolution and geopolymer gel formation.

It can be observed that the synthesized sodalite phase is relatively alkali-resistant [27]; the initial content of sodalite 3.5 and 5 wt% was only slightly reduced to 2.6 and 3.9 wt%, respectively. The maximum dissolved amount after 28 days is 25.7 %, obviously lower when compared to the results reported by Baykara et al. [42] who observed that the modernite dissolution varied from 30 to 60 wt%. This confirms the relatively high stability of sodalite synthesized in this study in a high-alkaline environment.

To understand the evolution of crystalline phases, specimens of three geopolymer pastes initially cured at 60 °C and finally stored at room temperature until the age of 28 days were heated at 400, 600, 800 and

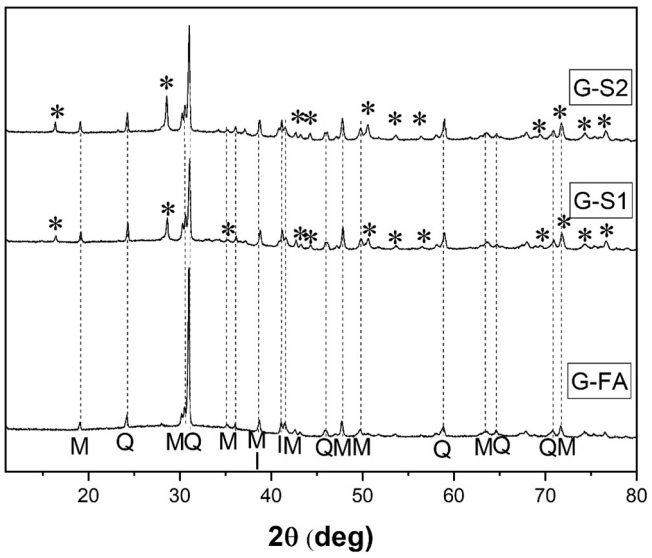

Fig. 5. XRD diffractograms of non-modified geopolymer paste (G-FA) and with sodalite-enrichment (G-S1 and G-S2) after 28 days, Legend: Q – quartz, M – Mullite, I – Iron (III) oxide, *-Sodalite; (detailed phase analysis shown in Table A (Appendix)).

1000 °C. Fig. 6 depicts a qualitative analysis of the findings, whereas Fig. 7 illustrates a quantitative explanation of the findings, including amorphous content variation. The analysis of the three prepared specimens revealed that the addition of sodalite influenced the phase formation in geopolymer at high-temperature. Fig. 6 demonstrates the maximum temperature of the measurement in which sodalite was identified. Lastly, Fig. 6 presents new thermally-induced crystalline phases, such as wollastonite, leucite, anorthoclase, nepheline or hematite. The maximum temperature where sodalite could still be identified was at 800 °C, which is similar to the findings of Bardez et al. [43]. This is due to the fact that changes in the range up to 900 °C are expected; however, the temperature measurement step (200 °C) did not allow for the precise determination of the temperature at which sodalite is no longer detected in XRD.

To better comprehend the nature of the aforementioned changes, a graphical depiction of the XRD Rietveld refinement was created (Fig. 7). In both G-S1 (Fig. 7b) and G-S2 (Fig. 7c), the amount of crystalline phase was increased, such as hematite, anorthoclase and leucite with the rise of the temperature, while G-FA underwent amorphization at above 800 °C which can be related to the melting process that lowered the stability of the matrix. In the sodalite free sample, decrease in amorphous phase up to 800 °C (77.6 wt% vs. 82.3 wt%) was observed due to the crystallization of hematite and nepheline. At temperatures above 900 °C the amorphous content increased again (80.4 wt%) due to the melting of mullite. In the sodalite samples, on the other hand, a continuous decrease in amorphous phase was observed due to the crystallisation of wollastonite, anorthoclase, nepheline and leucite.

The crystalline phases that have been identified in the sodalite-enriched samples are wollastonite and two feldspars anorthoclase and leucite. During the hydrothermal reaction of fly ash with NaOH, calcium appears to have been released and enriched the binder phase [44]. Non-new calcium-barring phases were identified in geopolymers but calcium enriched gel in the presence of chlorides did enhance the wollastonite formation [45]. Wollastonite can be originally identified (<1.0 wt%) in fly ash [46] and the analysed fly ash contained 0.6 wt% of wollastonite phase. However, in the geopolymer composites, G-S1 and G-S2 wollastonite had become more intensified after thermal exposure at above 600 °C, 2.3 wt% and 2.8 wt% respectively, which can be explained by the presence of chloride from sodalite decomposition that can influence wollastonite formation by lowering its crystallization temperature from 900 to 700 °C [44,46]. Chloride ions can influence the interaction between silica and calcium present in the matrix and direct the formation of wollastonite. In this temperature range, the amorphous calcium silicates underwent melting, which made the matrix more homogenous, thus the calcium ions were well-distributed in the matrix and could react with chloride providing the crystallization of wollastonite [47]. Along with the increase in the amount of sodalite from 3.5 to 5 wt% in the initial composition, an increase in the amount of wollastonite at 800 °C, 2.3 and 2.8 wt%, respectively was observed, while the reference showed the same wollastonite content (1.0 wt%).

In the geopolymer sample of G-S1 and G-S2, the formation of anorthoclase ($(Na,K)AlSi_3O_8$) and a minor amount of leucite ($KAlSi_2O_6$) was driven by the sodalite decomposition. Anorthoclase is a potassium- and sodium-bearing feldspar whose presence is linked to both the potassium-based activator and the sodium-rich product of hydrothermal reaction. Mouiya et al. [48] reported that the potassium-containing minerals such as anorthoclase are easily embedded in molten silicate formed in the temperature range 700–800 °C via dehydration and recrystallization. The quantified amount can be correlated to the initial amount of sodalite in the specimens. Leucite, the additional felspar, was formed as a result of sodalite decomposition by the reaction of K_2O with free SiO_2 coming from the sodalite. The amount of free silica and exposure temperature direct the content of leucite [49].

Furthermore, a small amount of halite was also formed due to the dissolution of sodalite and the presence of potassium ions in the glass phase. An interesting phenomenon is related to the nepheline crystallization at above 800 °C. Based on previous research [50–51], it was expected that the amount of nepheline would increase as a result of the sodalite decomposition, however, in this study sodalite promoted formation of two thermally stable phases such as anorthoclase (6.6 wt% G-S2) and wollastonite (2.8 wt% G-S2). Moreover, the highest amount of nepheline at 1000 °C was detected in the reference (0.7 wt%) while G-S1 and G-S2 possessed 0.4 wt% and 0.13 wt% respectively. Noteworthy, the formation of the nepheline phase which is associated with a volume expansion as shown by Stjernberg et al. particularly in the range 650 to 750 °C, which can cause volumetric instability and formation of cracks [52–53]. Thus, it can be assumed that sodalite improved thermal stability of the paste by promoting the formation of more stable phases. Nepheline formation may result from the disintegration of mullite above 600 °C from 10.4 wt% to 5.9 wt% for the reference material, due to the reaction of this phase with the surrounding matrix [54]. In every sample irrespectively to the sodalite enriching, the amount of quartz and anatase remained stable. Moreover, the increased content of iron oxide was explained by the opening of the unreacted fly ash spheres at above 600 °C [55], as well as dehydroxylation of amorphous iron oxides and formation of hematite initiated above 400 °C [56].

3.2. Thermogravimetric analyses (TG-DSC)

The TG results (Fig. 8) showed that the geopolymer had a continuous mass loss at elevated temperature, and the cumulative mass loss at 1000 °C of G-FA, G-S1, and G-S2 was 6.14, 6.71, and 7.36 %, respectively. Each sample showed similar mass loss at temperatures ranging from 40 °C to 100 °C due to the loss of the remaining physically bound water which should be removed during hydration stoppage. Moreover, the initial dehydration of hydrated aluminosilicate species and polycondensation occurred above 100 °C [1]. Above 300 °C, the mass loss was attributed to the release of chemically bound water and decomposition of metal-OH groups from sodalite [58]. The increase of the gradual weight loss between 300 °C and 700 °C (Fig. 8) was related to sodalite enrichment and was associated with dehydroxylation of the chemically bound group of silicon-hydroxyl and polymerization [59]. For sodalite enriched pastes, the shift of the weight loss to a higher temperature range (300–1000 °C) was associated with the dehydration of the sodalite structure and the transformation of sodalite to other aluminosilicates. Note that, hydrothermally synthesized chlorosodalite

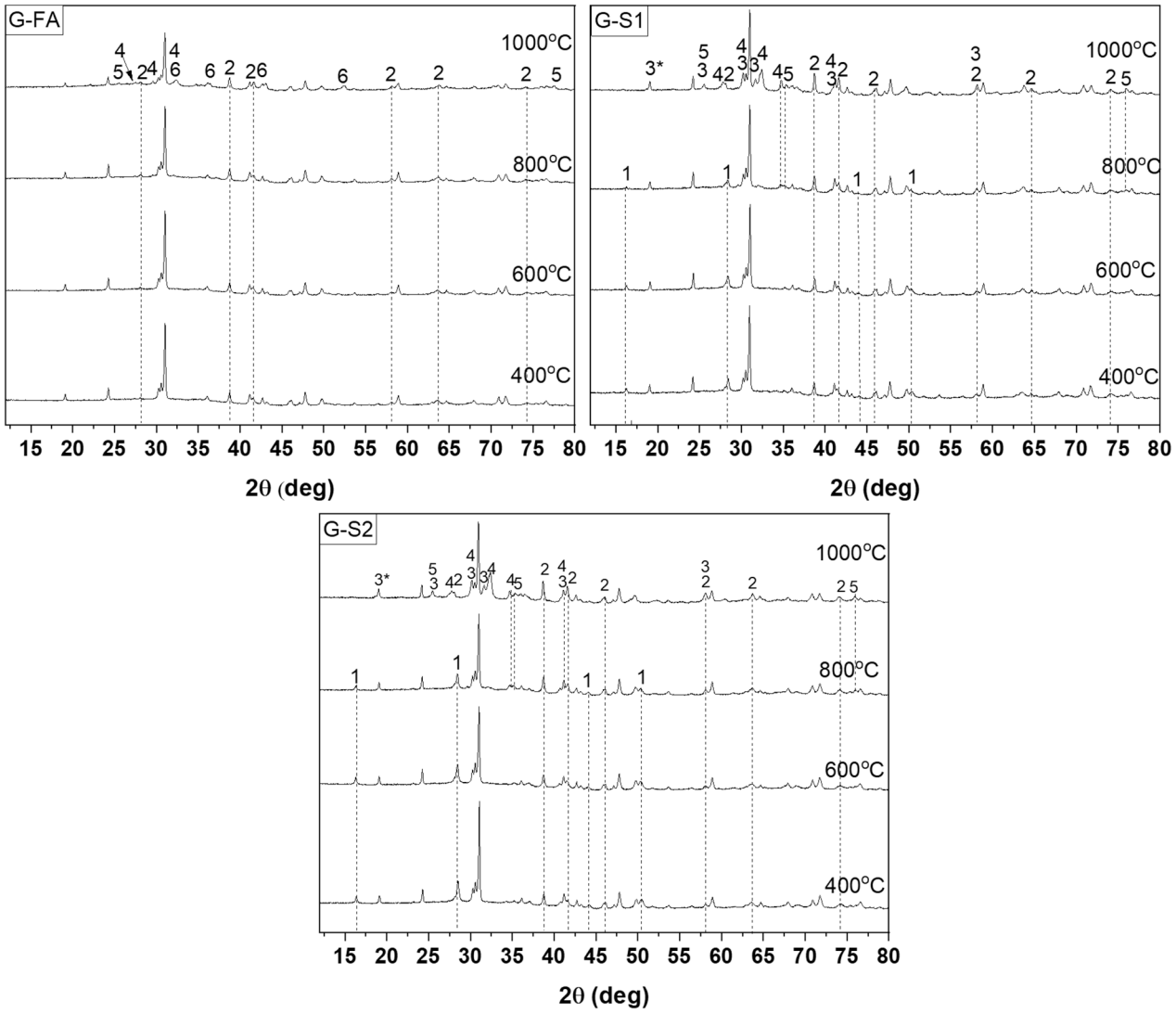

Fig. 6. XRD diffractograms of geopolymer pastes after high-temperature exposures with marked only new appeared phases and sodalite. Legend: 1. Sodalite; 2. Hematite; 3. Leucite; 3* overlapping peak of mullite and leucite; 4. Anorthoclase; 5. Wollastonite; 6. Nepheline.

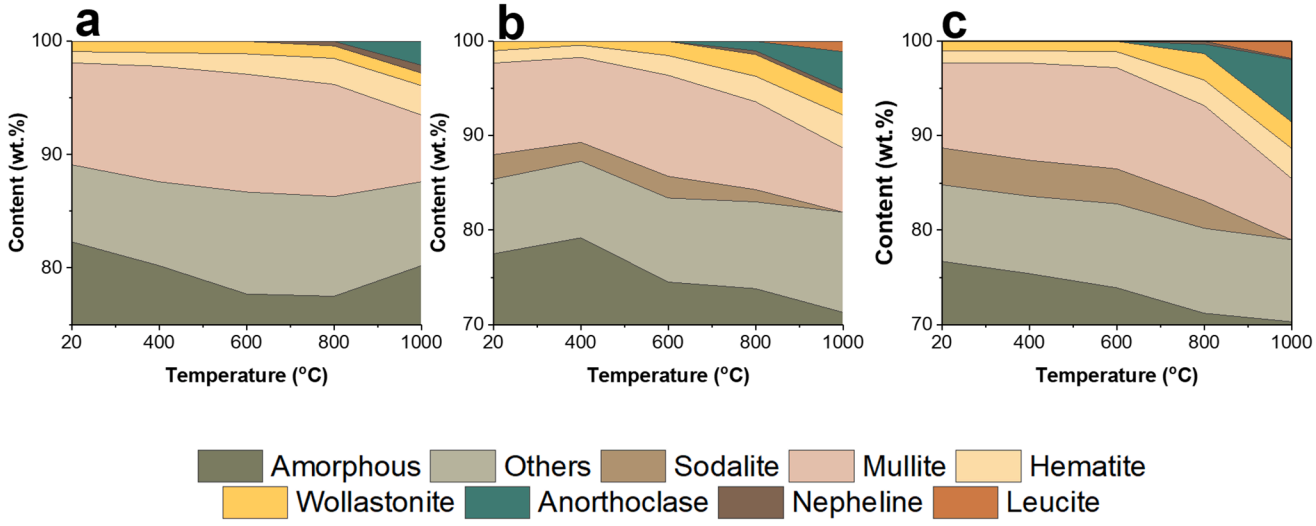

Fig. 7. XRD quantification of main phases in geopolymeric composites: a) G-FA; b) G-S1; c) G-S2.

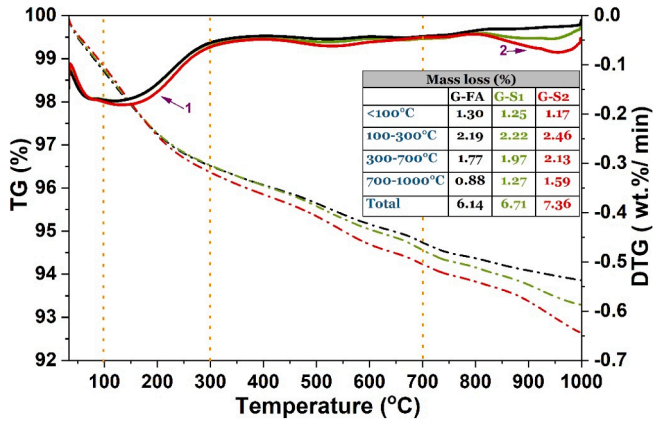

Fig. 8. TG curves of the composites after 28 days of curing. The table presents the mass loss in the specific temperature range (note: curve G-S1 and G-S2 overlaps). 1) loss of chemically bound water [57]; 2) slow halite decomposition and dehydroxylation associated with carbonate release from sodalite-rich material.

contains a small amount of hydroxysodalite, as indicated in XRD analysis, and this phase underwent multiple-step dehydration and dehydroxylation [60]. Hydroxysodalite phase increased the mass loss up to 700 °C and increased with the increased sodalite addition. Above 700 °C the mass loss can be assigned to further dehydroxylation of sodalite structure and chlorines volatiles until complete decomposition of this crystalline phase.

DSC (Fig. 9) is applied to present the reactions that took place during the tested temperature range. The DSC curve provided information about simultaneous (re)-crystallization and amorphization of the structures. The general observation of the DSC irrespective of the sodalite addition revealed a significant peak at around 150 °C, which was attributed to the gel decomposition. The observed peak shift between samples indicated the differences between water molecules binding with the matrix structures.

In the hump of glass transition (Fig. 9 grey area), the peak for G-S1 and G-S2 is shifted slightly towards lower temperature which suggested the decomposition of sodalite that affects the glass transition temperature. As a decomposition product, the amorphous phase was enriched by chlorine and sodium present in the sodalite structure. The sodium oxide which was incorporated into the glass phase lowered the temperature of softening and further influenced the formation of anorthoclase and the chloride determined wollastonite and halite formation, as discussed in the XRD analysis. It can be concluded that sodalite embedded in the matrix influenced the glass composition and its melting temperature,

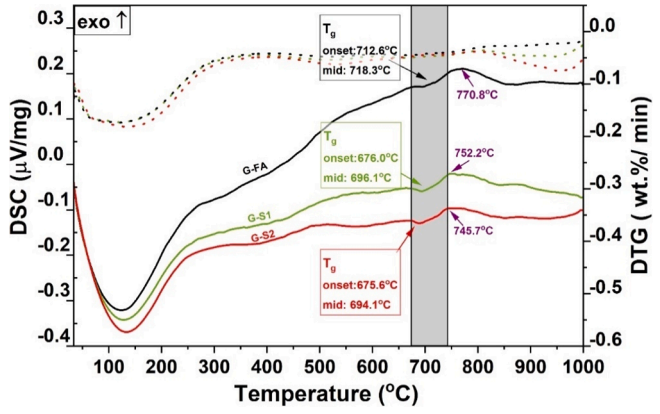

Fig. 9. DSC curves and glass transition determination of the samples combined with DTG curves (dotted-line). Grey area indicated the endothermic peak detected in each material.

mostly by the enriching system into sodium ions.

3.3. Scanning electron microscopy and optical microscope

The microscopic observations were carried out to further observe the effect of sodalite addition on the geopolymer composite. At room temperature, the geopolymer matrix appeared similar; the additional spherical particles in Fig. 10 G-S2 may be sourced from the post-reaction material from the hydrothermal process, as seen in Fig. 1. The agglomerates formed by sodalite crystals (also see Fig. 1) would influence the composite porosity.

Further thermally-induced fly ash particle dissolution and formation of geopolymeric gel at 400 °C caused the phenomenon of sodalite crystallites embedding in a newly developed geopolymer gel, could positively affect the homogenization of the matrix and increase the strength in this temperature range. This phenomenon occurs when water vapour and elevated temperature creates an autoclave condition boosting further geopolymerization reactions [61–62]. This possible phenomenon of coating the sodalite surface by geopolymer might additionally limit the access to the pores that distinguished the sodalite-enriched material. Furthermore, the stability of sodalite crystals in the matrix after high-temperature exposure at 800 °C was confirmed (Fig. 11). As mentioned in the various analyses, temperature above 700 °C defined the region of initiation of sodalite decomposition, but its durability can be defined in the range of 800–900 °C, allowing crystallites to be detected in both SEM and XRD analyses.

After exposure to 1000 °C (Fig. 12), the geopolymer gel showed clearly pores and channels and became more homogeneous and smoother due to viscous sintering. G-FA possessed a less porous structure with a predominance of closed pores, while in G-S1 and G-S2 it was possible to identify pore, voids, and channels. Furthermore, a clear difference in the colour of the reference sample's outer and inner parts were observed by the optical microscope. The observed reduced porosity of G-FA compared to G-S1 and G-S2, or the presence of closed pores, indicated intense melting and loss of material stability in the direction from the surface to the central part of the sample, resulting in limited oxidation processes in its interior and the characteristic dark area suggested a reduction environment.

3.4. Mercury intrusion porosimetry

The cumulative porosity and pore size distribution results were presented in Figs. 13 and 14, respectively. The cumulative porosity confirmed the hypothesis that the addition of sodalite led to an increase in pore volume, which was associated with the meso-macroporous sodalite, as revealed by BET (Fig. 2), as well as the formation of sodalite agglomerates (Fig. 11) which additionally influenced the pore volume [63]. In both samples G-S1 and G-S2 at 20 °C, the presence of sodalite was confirmed via an obvious peak shift towards a smaller pore size (~5.5 nm), which identified mesopores coming from sodalite-rich material (Fig. 2). Besides, the higher peak for G-S2 agreed with the higher amount of sodalite addition. Furthermore, at 400 °C the peak around 19 nm was observed for samples G-S1 and G-S2 that was not observed in G-FA, which was in agreement with sodalite crystals with a dominant spectrum of porosity between 12 and 22 nm [28]. Moreover, the increase in pore throat size after exposure to 400 °C may be due to overlapping processes; the sodium-enriched system had a smaller pore size than the pure potassium-based system [64]. Besides, up to the temperature of 400 °C, the further geopolymerization was triggered, and fly ash particles reacted in a series of reactions, sticking to the sodalite crystals, embedding them in an increasingly homogeneous geopolymer structure, as observed in SEM analysis. Simultaneously, the increase in the cumulative volume was observed which resulted from the formation of connections between pores and opening closed pores [64]. The pore size was characterized by a wider range of pores that corresponded to the potassium-based activation [65], whereas mesoporosity was primarily

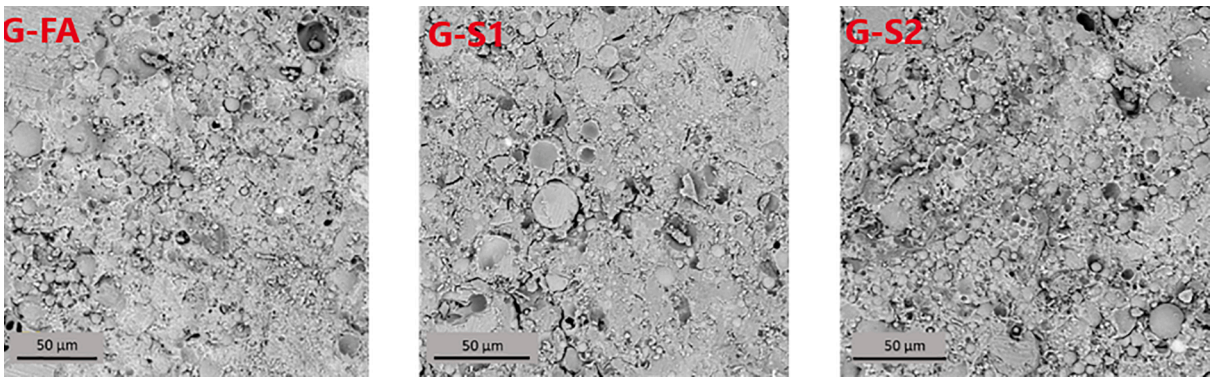

Fig. 10. SEM micrographs of geopolymer pastes at room temperature.

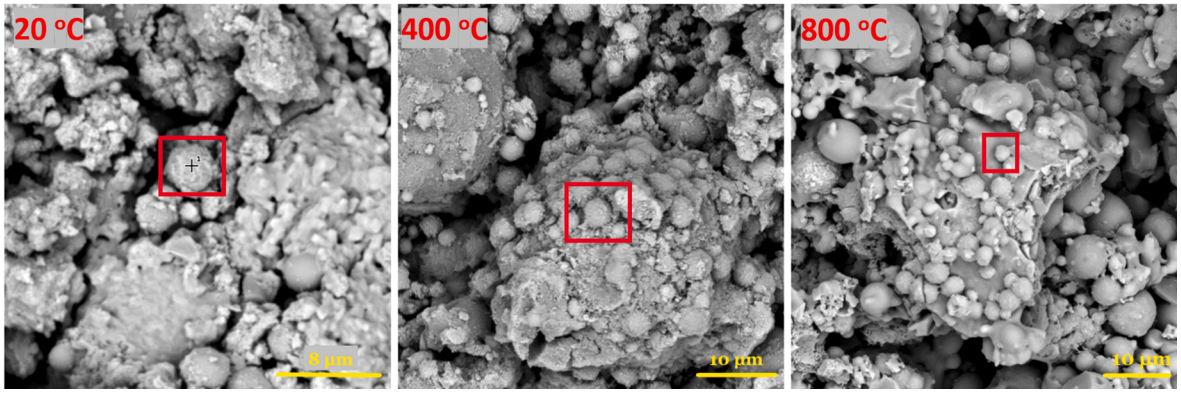

Fig. 11. Sample G-S2 at various temperatures. The red rectangle was marked with sodalite crystals (identification confirmed by EDS analysis).

due to the voids in the geopolymeric gel structure. Furthermore, the pore size (above 50 nm) could be related to the gaps between unreacted fly ash particles, regardless of the sample type. Moreover, a similar evolution of pore size distribution was also observed up to 600 °C due to the thermally-influenced processes, where the cumulative pore volume and the pore size increased via small size cracks, the opening of closed pores, improving the interconnectivity and pore throat [66]. Irrespective to the sodalite-addition, more prominent changes at 800 °C were observed when the peak in a small region was flattened and the curve shifted towards large pores, which were the result of crystallization and thermally induced macropores formation. However, it should be emphasized that differences existed in the porous structure, despite the above-mentioned similarities. For sodalite-enriched pastes, the phase composition at high temperature, and more specifically, the formation of anorthoclase, nepheline, and leucite might partially influence the reduction of the total porosity and the reduction of pore size. An additional role was played by the melting phenomenon, with the initiations determined by the DSC analysis. Although the sodalite-containing material was characterized by a lower glass transition temperature, which was also reflected in the reduced cumulative pore volume G-S2 and less significantly in G-S1 (Fig. 13), the sodalite-enhanced system did not suffer so much porosity degradation in the 800–1000 °C range. At 1000 °C, a distinct direction of microstructure transition between reference and G-S2 was visible.

Furthermore, between 800 and 1000 °C, sodalite-enriched specimens showed continuous pore size increase with an insignificant change in small size pores up to 5 µm. Apart from that the macropores peak was shifted towards larger pore size due to the conjoining of existing big size pores. Above 800 °C, G-FA started to lose thermal stability, which became the most prominent after exposure to 1000 °C. Dramatical structure densification at above 800 °C was due to the liquid formation, which indicated the loss of thermal stability of the geopolymer (porosity reduced from 44 to 13 %) [65], which was in agreement with the XRD quantification analysis, SEM, and optical microscope observations. This significant porosity decrease was not observed in sodalite-enriched samples, which supported the finding of improved performance of sodalite-geopolymer composite at high temperature.

3.5. Mechanical performance and volumetric deformation

The compressive strength and volumetric change of the samples after different temperature exposures were shown in Fig. 15. It can be seen that the reference sample showed higher compressive strength as a result of lower porosity compared to sodalite-containing samples (Fig. 13). However, a higher volumetric stability was shown in sample G-S1 and G-S2 thanks to the sodalite enrichment. In the temperature range from 20 to 600 °C, all the analyzed samples showed a similar trend. The noticeable increase in strength after exposure to 400 °C was attributed to the matrix densification, which also resulted in comparable volumetric deformation because of condensation reactions of the hydroxyl groups [66–67]. At 600 °C, strength reduction was observed as a result of simultaneously coexisting two phenomena, namely porosity increase and crystallization, which was in favour of the reduction of the amorphous part of the gel (Fig. 7). At 800 °C, a further strength increase was seen in G-S1 and G-S2, which was driven by the sodalite decomposition, pore volume maintained (G-S1) or decreased (G-S2), and formation of new crystalline products, such as anorthoclase and wollastonite. At the same time, as noted in the MIP and DSC analyses, a temperature of around 700 °C is the point at which glass transition is more significant in modified samples. The glass formation and cooling resulted in porosity decrease at 800 °C and strength increase by particle-binding effect. A minor influence can be also related to the formation of anorthoclase, whose small particles filled the small pores improving mechanical performance and wollastonite formation, which was

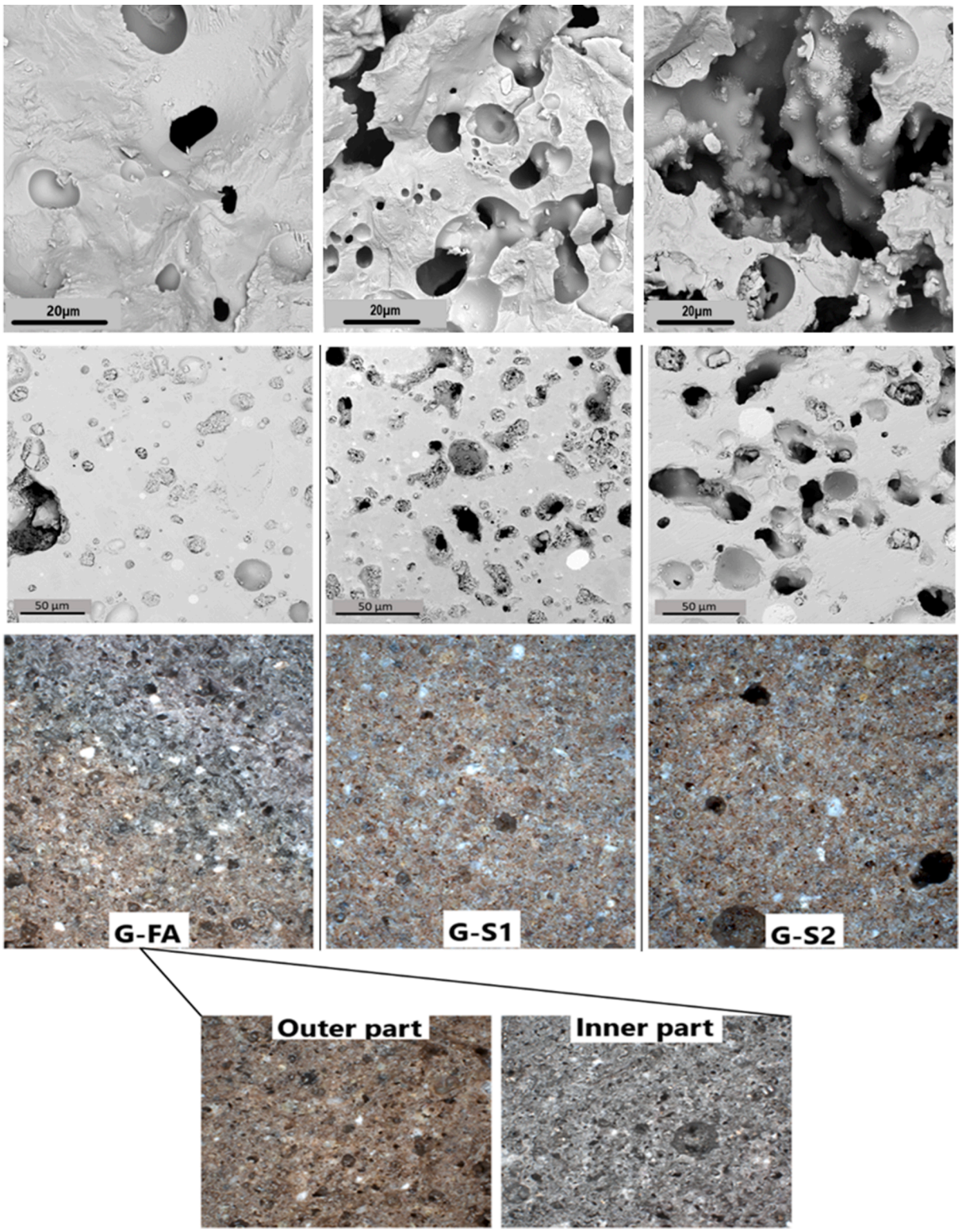

Fig. 12. SEM micrographs and optical microscope pictures of geopolymer pastes after exposure to 1000 °C.

confirmed as the promoter of mechanical strength by improving the tensile properties [68]. All geopolymer specimens showed further shrinkage evolution due to the structure densification [56,69], which however was more prominent in the non-enriched specimen. The considerable rise in shrinkage observed between 800 and 1000 °C in G-FA is due to the continued viscous sintering, which causes more dramatic porosity decrease, thermal shrinkage, but also continuous homogenization of the matrix. Furthermore, G-S1 and G-S2 modified samples have a higher proportion of crystalline phases (Fig. 7a), which, as observed by Vickers et al. [70], act as 'intrinsic fillers' and may contribute to shrinkage reduction. At 1000 °C, G-FA has a large proportion of amorphous phase, making it more susceptible to melting events. Lin et al. [71] observed a dramatic shrinkage of a highly amorphous metakaolin-based geopolymer at elevated temperatures, implying

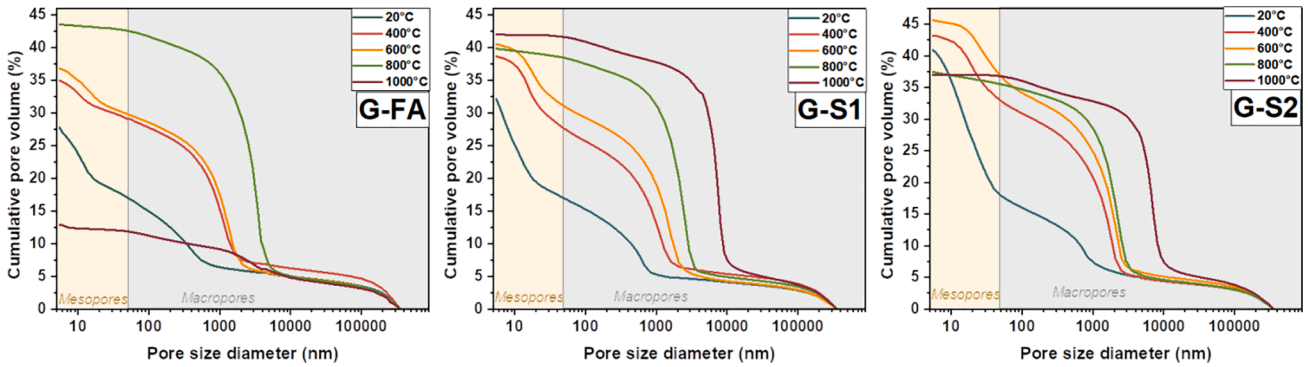

Fig. 13. Cumulative pore volume derived from Mercury Intrusion Porosimetry of the pastes after high temperature exposure.

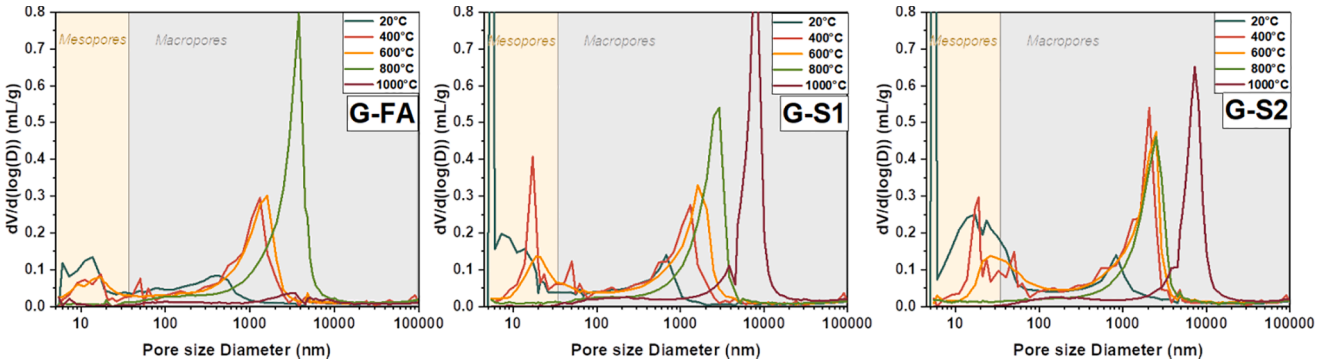

Fig. 14. Differential pore size distribution in the pastes after high-temperature exposure.

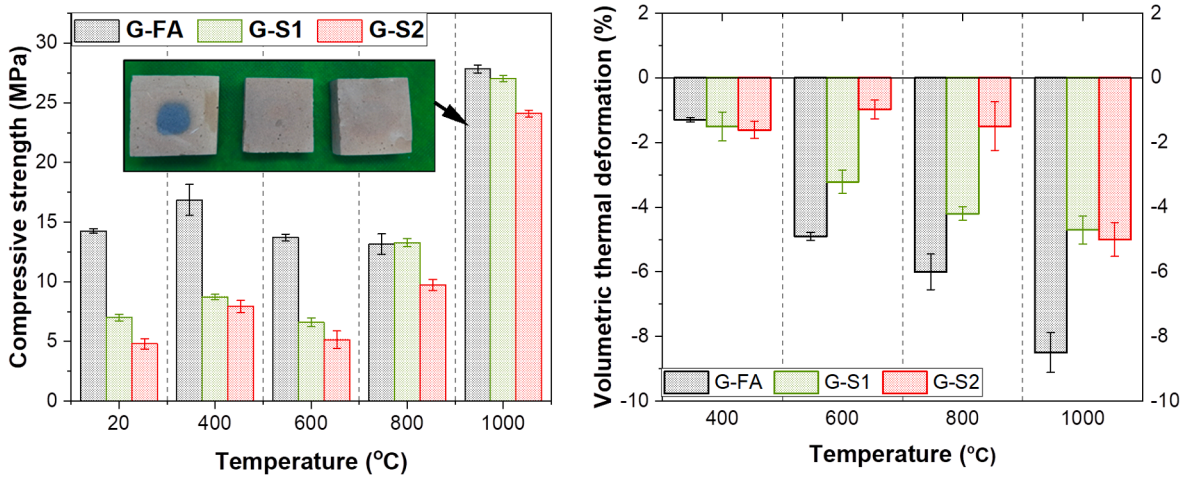

Fig. 15. Compressive strength evolution and volumetric deformation of the geopolymer specimens at different temperatures.

that an amorphous geopolymer structure reinforced by thermally resistant crystals is beneficial for volumetric thermal stability of the composite.

Viscous sintering at high temperature affected the macropores formation, volumetric shrinkage, and strength increase. At 400 °C, regardless of the sodalite addition, all specimens were characterized by the volumetric shrinkage in the range of 1.5 % that was resulted from the degradation of the geopolymer gel. Afterward, the shrinkage of G-FA in the range of 400 to 1000 °C tended to be linear. One of the reasons for this phenomenon was the melting process, which was also responsible for a significant decrease in porosity at 1000 °C. The overall sodalite-enriched materials showed less shrinkage over the entire temperature range.

However, attention should be paid to changes in individual temperature ranges and it can be noted that sodalite played a special role up to a temperature of 800 °C, which was associated with its decomposition. Although the temperature at which the decomposition started was about 700 °C, taking into account the quantitative distribution, it was be observed that between 600 and 800 °C the percentage of sodalite reduction (0.8 wt% for G-S2) was lower than that between 800 and 1000 °C (2.9 wt% for G-S2). It has been therefore also possible to deduce a significant decrease in the volume of G-S2 between 800 and 1000 °C. This contraction was also affected by the change in the composition of the vitreous phase and its sodium enrichment. The noticeable lower shrinkage was due to the different compositions of the crystalline phases, the crystallization of which may reduce the negative effects of the

melting. The lower degree of degradation may also confirm the different porosity of the composite after exposure to 1000 °C and, more precisely, the less noticeable reduction of the cumulative pore volume of G-S1 and G-S2 compared to G-FA.

In addition, after the compressive strength measurement, the resulting material residues were polished to show differences in the appearance of the cross-section (Fig. 15). It should be noted that the size of the polished specimens did not reflect the actual size of the composite due to the destructive nature of the strength test. The main observation, as pointed in Figs. 11 and 14, the cross-sections showed the difference in colour of the central part of the G-FA, while the core parts of the G-S1, G-S2, and outer part of G-FA had a characteristic brown-orange colour. This colour was due to the presence of iron oxide that underwent oxidation to hematite. The inner part of G-FA in black and grey indicated the lack of oxygen and the reduced conditions inside the material. As a result of the melting, the collapsing pores and the connections between them prevented air from entering the sample and caused thermal-induced transformations in the oxygen-deficient environment. Therefore, this observation confirmed that enrichment with sodalite had a beneficial effect on the reduction of volumetric shrinkage, especially up to the temperature of 800 °C.

4. Conclusions

The present study investigates enriching geopolymer matrix with thermally- and alkaline- stable crystalline particles to improve its high-temperature properties. This research leads to a better understanding of the thermal behaviour of ex-situ synthesized zeolite in geopolymer matrix, its influence on phase composition, porosity evolution and volumetric changes. Based on the obtained results, the main conclusions are drawn as follows:

- Sodalite addition influences the gel composition and thus the high temperature stability. Between the reference material and the sample with 5 % of sodalite addition, the temperature of the transition was lowered from 718.3 to 694.1 °C. This phenomenon was affected by the alkali ions which primarily defines the liquefaction point, namely the melting point of potassium aluminosilicate glass is greater than that of potassium-sodium mixed glass.
- The sodalite-enriched paste differs under high-temperature conditions on the formation of the crystalline stage. Noticeable formation of stable thermal anorthoclase, wollastonite, and a small amount of leucite is observed. These differences are more significant in specimens with 5 wt% sodalite addition and are attributed to the slow disintegration of sodalite at 800 °C and the greater decomposition observed between 800 and 1000 °C.
- The mesoporous nature of the raw material rich in sodalite contributes to the increased content of mesopores of geopolymer paste which reduces the deteriorating structural impact of water evaporation that passes through the material during heating.
- The synthesized sodalite-enriched material plays the role of a skeleton that facilitates the transport of evaporable water and significantly counteracts the harmful effects of volumetric deterioration by up to 800 °C (e.g. from 6 wt% for non-modified to 1.5 wt% for specimen enriched by 5 wt% of sodalite).
- The different strength evolution of geopolymer without and with sodalite results from a different path of porosity evolution between 400 and 800 °C and different phase composition at high temperature. The formation of new high-temperature stable crystalline from the sodalite-enriched matrix, such as anorthoclase and wollastonite which are embedded in the matrix at elevated temperature positively influence the strength performance of cooled geopolymer after temperature exposure.

Declaration of Competing Interest

The authors declare that they have no known competing financial interests or personal relationships that could have appeared to influence the work reported in this paper.

Acknowledgements

This research was carried out under project number S17013a in the framework of the Partnership Program of the Materials innovation institute M2i (www.m2i.nl) and the Technology Foundation TTW, which is part of the Netherlands Organization for Scientific Research (www.nwo.nl).

Appendix

A. Qualitative and quantitative analysis of raw materials and pastes at ambient temperature (errors show in the brackets)

Phase	Fly Ash	Sodalite-rich product	G-FA	G-S1	G-S2
Amorphous	78.1 (0.66)	45.1(0.61)	82.2 (0.43)	77.4 (0.60)	76.7 (0.50)
Mullite	11.3 (0.25)	10.8 (0.17)	9.0 (0.17)	9.7 (0.20)	9.0 (0.17)
Quartz	7.09 (0.16)	4.0 (0.08)	5.1 (0.10)	6.1 (0.12)	6.6 (0.14)
Hematite	1.4 (0.13)	1.1 (0.08)	1.0 (0.1)	1.3 (0.13)	1.3 (0.09)
Magnetite	0.6 (0.10)	0.2 (0.06)	0.7 (0.08)	0.5 (0.09)	0.2 (0.06)
Anatase	0.2 (0.05)	0.1 (0.03)	0.2 (0.04)	0.1 (0.04)	0.11 (0.03)
Periclase	0.2 (0.10)	0.5 (0.11)	0.3 (0.08)	0.7 (0.09)	0.5 (0.08)
Wollastonite	0.6 (0.46)	0.7 (0.28)	0.9 (0.32)	1.0 (0.44)	1.0 (0.33)
Pyrrhotite	0.3 (0.08)	0.4 (0.06)	0.2 (0.06)		
Calcite	0.3 (0.09)	0.8 (0.11)	0.4 (0.08)	0.7 (0.09)	0.5 (0.07)
Sodalite group		36.3 (0.24)		2.6 (0.14)	(0.15)

B. Qualitative and quantitative analysis of sample G-FA at elevated temperature

	400°C	600°C	800°C	1000°C
Amorphous	80.1 (0.39)	78.3 (0.48)	77.6 (0.56)	80.4 (0.43)
Mullite	10.2 (0.17)	10.5 (0.19)	9.9 (0.22)	5.9 (0.20)
Quartz	5.7 (0.11)	6.7 (0.12)	7.3 (0.13)	5.7 (0.11)

(*continued on next page*)

(*continued*)

	400°C	600°C	800°C	1000°C
Hematite	1.2 (0.11)	1.8 (0.11)	2.3 (0.13)	2.6 (0.12)
Magnetite	0.8 (0.08)	0.3 (0.06)	0.4 (0.09)	0.2 (0.07)
Anatase	0.1 (0.03)	0.1 (0.03)	0.2 (0.05)	0.2 (0.05)
Periclase	0.3 (0.08)	0.3 (0.09)	0.3 (0.09)	
Wollastonite	1.0 (0.23)	1.1 (0.35)	1.1 (0.4)	1.1 (0.18)
Pyrrhotite	0.2 (0.07)	0.3 (0.07)	0.3 (0.08)	0.9 (0.09)
Calcite	0.4 (0.08)	0.6 (0.08)	0.3 (0.08)	0.2 (0.07)
Nepheline			0.4 (0.13)	0.7 (0.13)
Anorthoclase				2.1 (0.13)

C. Qualitative and quantitative analysis of sample G-S1 at elevated temperature

	400°C	600°C	800°C	1000°C
Amorphous	79.2 (0.32)	74.6 (0.54)	74.0 (0.43)	72.5 (0.62)
Sodalite	2.0 (0.09)	2.3 (0.11)	1.3 (0.09)	
Mullite	9.0 (0.15)	10.7 (0.20)	9.3 (0.17)	6.9 (0.22)
Quartz	6.2 (0.08)	7.0 (0.12)	6.9 (0.1)	7.1 (0.13)
Hematite	1.3 (0.12)	2.1 (0.11)	2.7 (0.13)	3.6 (0.13)
Magnetite	0.6 (0.08)	0.1 (0.07)	0.5 (0.09)	0.6 (0.08)
Anatase	0.2 (0.04)	0.1 (0.04)	0.1 (0.04)	0.2 (0.06)
Calcite	0.6 (0.08)	0.5 (0.09)	0.5 (0.09)	0.1 (0.07)
Periclase	0.5 (0.09)	0.8(0.1)	0.6 (0.09)	0.6 (0.11)
Wollastonite	0.4 (0.24)	1.5 (0.40)	2.3 (0.18)	2.3 (0.23)
Halite potassian		0.3 (0.03)	0.3 (0.03)	0.4 (0.04)
Anorthoclase			1.0 (0.12)	4.1 (0.19)
Nepheline			0.4 (0.13)	0.4 (0.16)
Leucite				1.1 (0.13)

D. Qualitative and quantitative analysis of sample G-S2 at elevated temperature

	400°C	600°C	800°C	1000°C
Amorphous	75.4 (0.48)	74.0 (0.50)	71.3 (0.44)	70.3 (0.47)
Sodalite	3.8 (0.10)	3.7 (0.10)	2.9 (0.09)	
Mullite	10.3 (0.19)	10.7 (0.19)	10.1 (0.18)	6.5 (0.19)
Quartz	6.4 (0.11)	6.8 (0.11)	6.8 (0.09)	7.2 (0.11)
Hematite	1.3 (0.12)	1.7 (0.12)	2.7 (0.13)	3.2 (0.12)
Magnetite	0.5 (0.09)	0.5 (0.09)	0.6 (0.09)	0.6 (0.07)
Anatase	0.1 (0.03)	0.1 (0.03)	0.1 (0.04)	0.1 (0.05)
Calcite	0.5 (0.08)	0.5 (0.08)	0.5 (0.09)	0.2 (0.06)
Periclase	0.7 (0.10)	0.7 (0.09)	0.6 (0.09)	0.3 (0.07)
Wollastonite	1.0 (0.37)	1.1 (0.37)	2.8 (0.18)	2.8 (0.23)
Halite potassian		0.2 (0.03)	0.3 (0.04)	0.3 (0.04)
Anorthoclase			1.0 (0.13)	6.6 (0.14)
Nepheline			0.3 (0.13)	0.1 (0.07)
Leucite				1.8 (0.12)

References

[1] P. Duxson, G.C. Lukey, J.S.J. van Deventer, Thermal evolution of metakaolin geopolymers: Part 1 - Physical evolution, J. Non Cryst Solids. 352 (52-54) (2006) 5541–5555.

[2] W.D.A. Rickard, C.D. Borstel, A. Van Riessen, The effect of pre-treatment on the thermal performance of fly ash geopolymers, Thermochim Acta. 573 (2013) 130–137, https://doi.org/10.1016/j.tca.2013.09.030.

[3] W.D.A. Rickard, G.J.G. Gluth, K. Pistol, In-situ thermo-mechanical testing of fly ash geopolymer concretes made with quartz and expanded clay aggregates, Cem Concr Res. 80 (2016) 33–43, https://doi.org/10.1016/j.cemconres.2015.11.006.

[4] M. Król, P. Rożek, D. Chlebda, W. Mozgawa, Influence of alkali metal cations/type of activator on the structure of alkali-activated fly ash – ATR-FTIR studies, Spectrochim. Acta - Part A Mol Biomol. Spectrosc. 198 (2018) 33–37.

[5] İ.İ. Atabey, O. Karahan, C. Bilim, C.D. Atiş, The influence of activator type and quantity on the transport properties of class F fly ash geopolymer, Constr. Build. Mater. 264 (2020) 120268, https://doi.org/10.1016/j.conbuildmat.2020.120268.

[6] P. Duxson, G.C. Lukey, J.S.J. van Deventer, The thermal evolution of metakaolin geopolymers: Part 2 - Phase stability and structural development, J Non Cryst Solids. 353 (22-23) (2007) 2186–2200.

[7] M. Ozawa, F.U.A. Shaikh, A study on spalling behaviour of geopolymer mortars using ring restraint test, Constr Build Mater. 279 (2021), https://doi.org/10.1016/j.conbuildmat.2021.122494.

[8] P. Rożek, M. Król, W. Mozgawa, Geopolymer-zeolite composites: A review, J. Cleaner Prod. 230 (2019) 557–579.

[9] A.S. Rahman, D.W. Radford, Evaluation of the geopolymer/nanofiber interfacial bond strength and their effects on Mode-I fracture toughness of geopolymer matrix at high temperature, Compos Interfaces. 24 (8) (2017) 817–831, https://doi.org/10.1080/09276440.2017.1279479.

[10] S.A. Bernal, J. Bejarano, C. Garzón, Gutiérrez R.M. De, S. Delvasto, E.D. Rodríguez, Performance of refractory aluminosilicate particle / fiber-reinforced geopolymer composites, Compos Part B 43 (4) (2012) 1919–1928, https://doi.org/10.1016/j.compositesb.2012.02.027.

[11] L. Vickers, W.D.A. Rickard, A. Van Riessen, Strategies to control the high temperature shrinkage of fly ash based geopolymers, Thermochim. Acta 580 (2014) 20–27, https://doi.org/10.1016/j.tca.2014.01.020.

[12] Yan S, Feng X, Yang Y, Xing P. Effects of high-temperature exposure on properties of lightweight geopolymer foams incorporating diatomite powders. Int J Appl Ceram Technol.

[13] V. Vaou, D. Panias, Thermal insulating foamy geopolymers from perlite, Miner. Eng. 23 (14) (2010) 1146–1151.

[14] J.G. Sanjayan, A. Nazari, L. Chen, G.H. Nguyen, Physical and mechanical properties of lightweight aerated geopolymer, Constr. Build. Mater. 79 (2015) 236–244.
[15] E. Prud'homme, E. Joussein, S. Rossignol, Use of silicon carbide sludge to form porous alkali-activated materials for insulating application, Eur Phys J Spec Top. 224 (9) (2015) 1725–1735.
[16] S. Yan, F. Zhang, X. Feng, J. Kong, B.o. Wang, J. Yang, Effect of high temperature on the mechanical properties of hierarchical porous cenosphere/geopolymer composite foams, Int. J. Appl. Ceram. Technol. 18 (3) (2021) 817–829.
[17] G. Franchin, P. Colombo, Porous geopolymer components through inverse replica of 3D printed sacrificial templates, J Ceram Sci Technol. (2015).
[18] E. Papa, V. Medri, P. Benito, A. Vaccari, S. Bugani, J. Jaroszewicz, et al., Synthesis of porous hierarchical geopolymer monoliths by ice-templating, Microporous Mesoporous Mater. (2015).
[19] C. Bai, P. Colombo, Processing, properties and applications of highly porous geopolymers: A review, Ceram. Int. 44 (14) (2018) 16103–16118.
[20] G. Roviello, C. Menna, O. Tarallo, L. Ricciotti, C. Ferone, F. Colangelo, D. Asprone, R. di Maggio, E. Cappelletto, A. Prota, R. Cioffi, Preparation, structure and properties of hybrid materials based on geopolymers and polysiloxanes, Mater. Des. 87 (2015) 82–94.
[21] A. Pfenninger, Manufacture and Use of Zeolites for Adsorption Processes, In (1999).
[22] A. Nikolov, I. Rostovsky, H. Nugteren, Geopolymer materials based on natural zeolite, Case Stud. Constr. Mater. 6 (2017) 198–205.
[23] C. Villa, E.T. Pecina, R. Torres, L. Gómez, Geopolymer synthesis using alkaline activation of natural zeolite, Constr. Build. Mater. 24 (11) (2010) 2084–2090.
[24] A.A. Shahmansouri, M. Nematzadeh, A. Behnood, Mechanical properties of GGBFS-based geopolymer concrete incorporating natural zeolite and silica fume with an optimum design using response surface method, J Build Eng. 36 (2021) 102138, https://doi.org/10.1016/j.jobe.2020.102138.
[25] D.W. Breck, Zeolite Molecular Sieves: Structure, Chemistry and Use, Anal. Chim. Acta (1975).
[26] Chong S, Program WSUMS and E. Characterization of Sodalite Based Waste Forms for Immobilization of 129I [Internet]. Washington State University; 2017. Available from: https://books.google.nl/books?id=o3PtvQEACAAJ.
[27] J. Luo, H. Zhang, J. Yang, Hydrothermal Synthesis of Sodalite on Alkali-Activated Coal Fly Ash for Removal of Lead Ions. Procedia, Environ Sci. 31 (2016) 605–614.
[28] W. Franus, M. Wdowin, M. Franus, Synthesis and characterization of zeolites prepared from industrial fly ash, Environ. Monit. Assess. 186 (9) (2014) 5721–5729.
[29] H. Beyer, Dealumination Techniques for Zeolites, In: Mol Sieves. (2002) 203–255.
[30] S. Khajavi, S. Sartipi, J. Gascon, J.C. Jansen, F. Kapteijn, Thermostability of hydroxy sodalite in view of membrane applications, Available from, Microporous Mesoporous Mater 132 (3) (2010) 510–517, http://www.sciencedirect.com/science/article/pii/S1387181110001046.
[31] S. Golbad, P. Khoshnoud, N. Abu-Zahra, Hydrothermal synthesis of hydroxy sodalite from fly ash for the removal of lead ions from water, Int. J. Environ. Sci. Technol. 14 (1) (2017) 135–142.
[32] J. Li, X. Zeng, X. Yang, C. Wang, X. Luo, Synthesis of pure sodalite with wool ball morphology from alkali fusion kaolin, Mater. Lett. 161 (2015) 157–159.
[33] J. Yang, T. Li, X. Bao, Y. Yue, H. Liu, Mesoporogen-free synthesis of hierarchical sodalite as a solid base catalyst from sub-molten salt-activated aluminosilicate, Particuology 48 (2020) 48–54.
[34] A.V. Borhade, S.R. Kankrej, An efficient cost-effective removal of Ca2+, Mg2+, and Cu2+ ions from aqueous medium using chlorosodalite synthesized from coal fly ash, J. Chem. Eng. Data 62 (2) (2017) 596–607.
[35] Sindhunata, J.S.J. van Deventer, G.C. Lukey, H. Xu, Effect of curing temperature and silicate concentration on fly-ash-based geopolymerization, Ind. Eng. Chem. Res. 45 (10) (2006) 3559–3568.
[36] P.V. Krivenko, G.Y. Kovalchuk, Directed synthesis of alkaline aluminosilicate minerals in a geocement matrix, J. Mater. Sci. 42 (9) (2007) 2944–2952.
[37] E. Papa, V. Medri, S. Amari, Jérémie Manaud, P. Benito, A. Vaccari, E. Landi, Zeolite-geopolymer composite materials: Production and characterization, J Clean Prod. 171 (2018) 76–84.
[38] T. Bakharev, Geopolymeric materials prepared using Class F fly ash and elevated temperature curing, Cem. Concr. Res. 35 (6) (2005) 1224–1232.
[39] Hardjito D, Rangan BV. Development and properties of low-calcium fly ash-based geopolymer concrete [Internet]. Research report GC. Perth; 2005 [cited 2012 Jun 13]. Available from: http://www.geopolymer.org/fichiers_pdf/curtin-flyash-GP-concrete-report.pdf.
[40] K. Scrivener, R. Snellings, B. Lothenbach, A practical guide to microstructural analysis of cementitious materials, Crc Press (2018).
[41] BSI. BS EN 196-1: 2005: Methods of testing cement. Determination of strength. BSI London, UK; 2005.
[42] H. Baykara, M.H. Cornejo, R. Murillo, A. Gavilanes, C. Paredes, J. Elsen, Preparation, characterization and reaction kinetics of green cement: Ecuadorian natural mordenite-based geopolymers, Mater. Struct. 50 (3) (2017) 188.
[43] I. Bardez, L. Campayo, D. Rigaud, M. Chartier, A. Calvet, M. Céramiques, et al., Investigation of sodalites for conditioning halide salts (NaCl and NaI). In: Nuclear fuel cycle for a sustainable future, 2008.
[44] J.L. Provis, V. Rose, S.A. Bernal, J.S.J. van Deventer, High-resolution nanoprobe X-ray fluorescence characterization of heterogeneous calcium and heavy metal distributions in alkali-activated fly ash, Langmuir 25 (19) (2009) 11897–11904.
[45] R.Guimarães. Ribas, T.M.B. Campos, V.M. Schatkoski, B.R.C. de Menezes, Thaís.L. do.A. Montanheiro, G.Patrocínio. Thim, α-wollastonite crystallization at low temperature, Ceram. Int. 46 (5) (2020) 6575–6580.
[46] S.V. Vassilev, R. Menendez, D. Alvarez, M. Diaz-Somoano, M.R. Martinez-Tarazona, Phase-mineral and chemical composition of coal fly ashes as a basis for their multicomponent utilization. 1. Characterization of feed coals and fly ashes☆, Fuel 82 (14) (2003) 1793–1811.
[47] X. Chen, N. Karpukhina, D.S. Brauer, R.G. Hill, High chloride content calcium silicate glasses, PCCP 19 (10) (2017) 7078–7085.
[48] M. Mouiya, A. Bouazizi, A. Abourriche, A. Benhammou, Y. El Hafiane, M. Ouammou, Y. Abouliatim, S.A. Younssi, A. Smith, H. Hannache, Fabrication and characterization of a ceramic membrane from clay and banana peel powder: Application to industrial wastewater treatment, Mater. Chem. Phys. 227 (2019) 291–301.
[49] L.A.M. Scudeller, E. Longo, J.A. Varela, Potassium vapor attack in refractories of the alumina–silica system, J. Am. Ceram. Soc. 73 (5) (1990) 1413–1416.
[50] D. Novembre, D. Gimeno, A. Pasculli, B. Di Sabatino, Synthesis and characterization of sodalite using natural kaolinite: An analytical and mathematical approach to simulate the loss in weight of chlorine during the synthesis process, Fresenius Environ. Bull. (2010).
[51] B.J. Riley, J.D. Vienna, S.M. Frank, J.O. Kroll, J.A. Peterson, N.L. Canfield, Z. Zhu, J. Zhang, K. Kruska, D.K. Schreiber, J.V. Crum, Glass binder development for a glass-bonded sodalite ceramic waste form, J. Nucl. Mater. 489 (2017) 42–63.
[52] J. Stjernberg, B. Lindblom, J. Wikström, M.-L. Antti, M. Odén, Microstructural characterization of alkali metal mediated high temperature reactions in mullite based refractories, Ceram. Int. 36 (2) (2010) 733–740.
[53] J. Stjernberg, M. Antti, L. Nordin, M. Odén, Degradation of refractory bricks used as thermal insulation in rotary kilns for iron ore pellet production, Int. J. Appl. Ceram. Technol. 6 (6) (2009) 717–726.
[54] S. Wattanasiriwech, F. Arif Nurgesang, D. Wattanasiriwech, P. Timakul, Characterisation and properties of geopolymer composite part 1: Role of mullite reinforcement, Ceram. Int. 43 (18) (2017) 16055–16062.
[55] W.D.A. Rickard, A. Van Riessen, P. Walls, Thermal character of geopolymers synthesized from class F fly ash containing high concentrations of iron and α-quartz, Int. J. Appl. Ceram. Technol. 7 (1) (2010) 81–88.
[56] P. Duxson, G.C. Lukey, J.S.J. Van Deventer, Physical evolution of Na-geopolymer derived from metakaolin up to 1000 °c, J. Mater. Sci. 42 (9) (2007) 3044–3054.
[57] A.M. El Nagar, H.M. Khater, Development of High Thermal Stability Geopolymer Composites Enhanced by Nano Metakaolin, J Build Mater Struct. 6 (1) (2019) 10–19.
[58] D.D. Burduhos Nergis, M.M.A.B. Abdullah, A.V. Sandu, P. Vizureanu, XRD and TG-DTA Study of New Alkali Activated Materials Based on Fly Ash with Sand and Glass Powder, Materials (Basel). 13 (2) (2020) 343, https://doi.org/10.3390/ma13020343.
[59] Q. Li, H. Xu, F. Li, P. Li, L. Shen, J. Zhai, Synthesis of geopolymer composites from blends of CFBC fly and bottom ashes, Fuel 97 (2012) 366–372.
[60] P. Sturm, G.J.G. Gluth, S. Simon, H.J.H. Brouwers, H.-C. Kühne, The effect of heat treatment on the mechanical and structural properties of one-part geopolymer-zeolite composites, Thermochim Acta 635 (2016) 41–58.
[61] Z. Pan, J.G. Sanjayan, B.V. Rangan, An investigation of the mechanisms for strength gain or loss of geopolymer mortar after exposure to elevated temperature, J. Mater. Sci. 44 (7) (2009) 1873–1880.
[62] I. Hager, M. Sitarz, K. Mróz, Fly-ash based geopolymer mortar for high-temperature application–Effect of slag addition, J Clean Prod. 316 (2021) 128168, https://doi.org/10.1016/j.jclepro.2021.128168.
[63] Khajavi S, Sartipi S, Gascon J, Jansen JC, Kapteijn F. Thermostability of hydroxy sodalite in view of membrane applications. Microporous Mesoporous Mater [Internet]. 2010;132(3):510–7. Available from: https://doi.org/10.1016/j.micromeso.2010.03.035.
[64] M. Lahoti, K.K. Wong, K.H. Tan, E.-H. Yang, Effect of alkali cation type on strength endurance of fly ash geopolymers subject to high temperature exposure, Mater. Des. 154 (2018) 8–19.
[65] T. Bakharev, Thermal behaviour of geopolymers prepared using class F fly ash and elevated temperature curing, Cem. Concr. Res. 36 (6) (2006) 1134–1147.
[66] M. Lahoti, S.F. Wijaya, K.H. Tan, E.-H. Yang, Tailoring sodium-based fly ash geopolymers with variegated thermal performance, Cem. Concr. Compos. 107 (2020) 103507, https://doi.org/10.1016/j.cemconcomp.2019.103507.
[67] L. Vickers, A. van Riessen, W. Rickard, Fire-resistant Geopolymers: Role of Fibres and Fillers to Enhance Thermal Properties, SpringerBriefs in Materials. (2015).
[68] M. Mouiya, A. Bouazizi, A. Abourriche, Y. El Khessaimi, A. Benhammou, Y. El hafiane, Y. Taha, M. Oumam, Y. Abouliatim, A. Smith, H. Hannache, Effect of sintering temperature on the microstructure and mechanical behavior of porous ceramics made from clay and banana peel powder, Results Mater. 4 (2019) 100028, https://doi.org/10.1016/j.rinma.2019.100028.
[69] W.D.A. Rickard, R. Williams, J. Temuujin, A. van Riessen, Assessing the suitability of three Australian fly ashes as an aluminosilicate source for geopolymers in high temperature applications, Mater. Sci Eng A. 528 (9) (2011) 3390–3397, https://doi.org/10.1016/j.msea.2011.01.005.
[70] W.D.A. Rickard, J. Temuujin, A. Van Riessen, Thermal analysis of geopolymer pastes synthesised from five fly ashes of variable composition, J. Non Cryst Solids. 358 (15) (2012) 1830–1839, https://doi.org/10.1016/j.jnoncrysol.2012.05.032.
[71] T.S. Lin, D.C. Jia, P.G. He, M.R. Wang, Thermo-mechanical and microstructural characterization of geopolymers with α-Al 2 O 3 particle filler, Int. J. Thermophys. 30 (5) (2009) 1568–1577.